Bioinspired Collagen-Apatite Nanocomposites for Bone Regeneration

Shuai Liu, PhD, Yue Sun, PhD,* Yu Fu,* Datong Chang, MD,* Cuicui Fu,† Gaonan Wang,* Yan Liu, PhD,* Franklin R. Tay, PhD,‡ and Yanheng Zhou, PhD**

Abstract

Introduction: Natural bone has a complex hierarchical nanostructure composed of well-organized collagen fibrils embedded with apatite crystallites. Bone tissue engineering requires scaffolds with structural properties and functionality similar to the natural bone. Inspired by bone, a collagen-apatite (Col-Ap) nanocomposite was fabricated with bonelike subfibrillar nanostructures using a modified bottom-up biomimetic approach and has a potential role in the healing of large bone defects in unresolved apical periodontitis. **Methods:** The bone regeneration potential of the Col-Ap nanocomposite was investigated by comparing it with inorganic beta-tricalcium phosphate and organic pure collagen using a critical-sized rodent mandibular defect model. Micro–computed tomographic imaging and histologic staining were used to evaluate new bone formation *in vivo*. **Results:** When compared with the beta-tricalcium phosphate and collagen scaffolds, the Col-Ap nanocomposite scaffold exhibited superior regeneration properties characterized by profuse deposition of new bony structures and vascularization at the defect center. Immunohistochemistry showed that the transcription factor osterix and vascular endothelial growth factor receptor 1 were highly expressed in the Col-Ap group. The results indicate that the Col-Ap nanocomposite activates more bone-forming cells and stimulates more vascular tissue ingrowth. Furthermore, the Col-Ap nanocomposite induces extracellular matrix secretion and mineralization of rat bone marrow stem cells. The increased expression of transforming growth factor beta 1 may contribute to the formation of a mineralized extracellular matrix. **Conclusions:** The present study lays the foundation for the development of Col-Ap nanocomposite–based bone grafts for future clinical applications in bone regeneration of large periapical lesions after apical curettage or apicoectomy. *(J Endod 2016;42:1226–1232)*

Key Words

Apatite, biomimetics, bone scaffold, collagen, histology, immunohistochemistry, *in vivo*, micro–computed tomography, nanocomposite

Significance

The collagen-apatite nanocomposite may be further developed for clinical applications in bone regeneration of large periapical lesions after apical curettage or apicoectomy wherein part of the surgical defect is blocked by the presence of a partially resected root.

Large bone defects associated with extensive unresolved apical periodontitis (1–3), particularly those with total loss of the buccal cortical plate (4, 5), may suffer from delayed healing or healing by granulation tissues after enucleation of extensive periradicular lesions and the use of root-end fillings to limit potentially noxious agents within the confines of the affected roots. Healing of these extensive surgical lesions may benefit from the use of bone substitutes and guided tissue regeneration to reverse the process of bone loss and to regenerate bone (6, 7). Traditional approaches to bone regeneration focus on the use of bone autografts, allografts, and xenografts. However, complications such as donor-site morbidity, host immune rejection, and disease transmission restrict the application of these tissue grafts. To circumvent the aforementioned limitations, synthetic biomaterials including ceramics, polymers, and composites have been developed as potential bone grafting materials (8).

Beta-tricalcium phosphate (β-TCP), a member of the calcium phosphate ceramics family, has been considered as a temporary scaffold for bone regeneration because of its similar mineral phase composition to human bone, biocompatibility, and osteoconductivity (9). Being a pure inorganic material, β-TCP lacks the flexibility of organic polymers and specific microstructures of bone, lacks osteoinductivity, and degrades slowly, resulting in slow *in vivo* bone formation (10). Microstructured composites, which consist of calcium phosphate microparticles and biodegradable polymers such as collagen (Col), offer an alternative solution to overcome some of these drawbacks (11). Because natural bone is a hierarchically structured nanocomposite comprising apatite crystallites dispersed within the Col matrix (12), nanocomposites with similar hierarchical structures may offer improved functional and biological properties compared with conventional microstructured biomaterials or composites in bone tissue engineering (13).

From the *Center for Craniofacial Stem Cell Research and Regeneration, Department of Orthodontics, Peking University School and Hospital of Stomatology, Beijing, People's Republic of China; †Department of Orthodontics, School of Stomatology, Zhengzhou University, Henan, People's Republic of China; and ‡Department of Endodontics, The Dental College of Georgia, Augusta University, Augusta, Georgia.

Address requests for reprints to Prof Yan Liu or Prof Yanheng Zhou, Center for Craniofacial Stem Cell Research and Regeneration, Department of Orthodontics, Peking University School and Hospital of Stomatology, 22# Zhongguancun South Avenue, Haidian District, Beijing, 100081, China. E-mail address: orthoyan@bjmu.edu.cn or yanhengzhou@vip.163.com

0099-2399/$ - see front matter

http://dx.doi.org/10.1016/j.joen.2016.04.027

A 2-dimensional collagen-apatite (Col-Ap) nanocomposite mimicking a bone hierarchical nanostructure was previously fabricated by the authors (14). This Col-Ap nanocomposite is biocompatible and possesses acceptable nanomechanical properties (15). However, the potential of the bioinspired 3-dimensional (3D) Col-Ap nanocomposite scaffold in regenerating new bone is unclear. In the present study, bone formation brought by *in vivo* implantation of the 3D Col-Ap nanocomposite scaffold was compared with that produced by a microstructured scaffold comprising β-TCP and pure Col using a critical-sized rodent mandibular defect model. The osteogenic ability of different scaffolds was also investigated *ex vivo*.

Materials and Methods

Scaffold Preparation

The 3D Col-Ap nanocomposite was prepared using a modified bottom-up biomimetic approach (14, 15) by reconstituting Col from a type I tropocollagen solution using simulated body fluid (16) as the phosphate source, white Portland cement (Lehigh Cement Co, Allentown, PA) as the calcium source, and polyacrylic acid (Mw 1800; MilliporeSigma, St Louis, MO) as the stabilizer of amorphous calcium phosphate (Supplemental Figures S1 and S2 are available online at www.jendodon.com). β-TCP scaffolds were prepared using porous β-TCP granules (ChronOS; Synthes, West Chester, PA). Col scaffolds were prepared by dialysis of the tropocollagen solution in 0.1 mol/L phosphate-buffered saline (PBS).

The 3 types of scaffolds were dehydrated in a graded series of ethanol (50%, 70%, 80%, 85%, 90%, 95%, and 100%), critical point dried, and observed with scanning electron microscopy (S-4800; Hitachi High-Technologies Corp, Tokyo, Japan) at 15 kV. Elemental analysis of the scaffolds was performed using energy-dispersive X-ray spectroscopy coupled to the scanning electron microscope. Cell-seeded scaffolds were washed 3 times with PBS and fixed in 2.5% glutaraldehyde in PBS before scanning electron microscopic examination.

Experimental Animals

Adult male Sprague Dawley rats obtained from the Department of Laboratory Animal Science, Peking University Health Science Center, Beijing, People's Republic of China, were housed in groups of 5 and given 1 week to acclimate to the housing facility. The rats were given access to rat maintenance food and water *ad libitum*. During housing, the rats were monitored twice daily for their health status. No adverse events were observed. Experimenters were blinded to the treatment during data processing. The study was performed in strict accordance with the recommendations in the guide for the Care and Use for Laboratory Animals of the National Institutes of Health. All protocols were approved by the Animal Use and Care Committee of Peking University (permit number: LA2014218). All surgeries were performed under sodium pentobarbital anesthesia; all efforts were made to minimize suffering.

Isolation and Identification of Rat Bone Marrow Stem Cells

Rat bone marrow stem cells (rBMSCs) were isolated from bone marrow specimens obtained by cutting off the femora from 3-week-old rats (90–100 g) (17). After flushing out with PBS, the cells were cultured in alpha minimum essential medium (Gibco, ThermoFisher Scientific, Waltham, MA) with 20% fetal bovine serum (Hyclone; GE Healthcare Life Sciences, Logan, UT), 100 U/mL penicillin/streptomycin, 2 mmol/L glutamine, 55 μmol/L 2-ME (Gibco), and 0.1 mmol/L L-ascorbic acid phosphate (Wako Chemicals, Richmond, VA) at 37°C in 5% CO_2. Multipotency of the rBMSCs was confirmed by examining osteogenicity using alizarin red S staining and adipogenicity using oil red O staining (Supplemental Figure S1*A–C* is available online at www.jendodon.com) (18).

Animal Experiments

Twenty 5-mm diameter, nonhealing full-thickness defects were created in the mandible of each of the 6- to 8-week-old rats (180–200 g) to evaluate the bone regeneration potential of different scaffolds (Supplemental Figure S1*D* is available online at www.jendodon.com) (19). Both the cortical bone and cancellous bone were removed from those defects. The Col-Ap nanocomposite, β-TCP scaffold (n = 5), and Col (n = 5) scaffold were randomly placed into the defect area without cell seeding or growth factor supplementation (n = 5); no scaffold was used in the negative control (n = 5). The wound was closed in layers using 6-0 sutures. Body temperature was maintained throughout the surgery using a homeothermic blanket system, and sterile saline irrigation was used during surgery. After 20 weeks of implantation, the rats were sacrificed by overanesthesia. The mandibles were obtained *en bloc* and fixed in 4% paraformaldehyde.

Micro–Computed Tomographic Imaging

The mandibles were scanned using micro–computed tomographic (micro-CT) imaging (Inveon MMCT; Siemens Medical Solutions, Knoxville, TN) at 80 kV and 500 μA. The Inveon Research Workplace software (Siemens) was used for 3D image reconstruction and calculation of the volume of the radiopaque area (gray value >1000).

Histologic Examination

After micro-CT scanning, each mandible was completely demineralized in 15% EDTA and embedded in paraffin. Five-micrometer-thick serial sections were obtained from the midsagittal plane of the defect area. Tissue sections were deparaffinized with xylene, dehydrated in a graded series of ethanol (70%–100%), stained with hematoxylin-eosin, and examined by light microscopy. Three sections from 1 individual sample were collected and used for quantification. Images of the defect margin and defect center were captured, and the ratio of new bone to the total area was evaluated using Image-Pro Plus software (Azure Biosystems, Inc, Dublin, CA). Measurements were repeated 3 times by a trained researcher who was blinded to the group designations.

Immunohistochemistry

Immunohistochemistry was performed with a 2-step detection kit (Zhongshan Golden Bridge Biotechnology, Beijing, China). Tissue sections (n = 5) in each group were subjected to antigen retrieval using 0.125% trypsin and 20 μg/mL proteinase K; blocked with 5% bovine serum albumin; and incubated overnight with antibodies against rat zinc finger transcription factor osterix (Osx, 1:800 [ab22552; Abcam, Cambridge, MA]), vascular endothelial growth factor receptor 1 (VEGFR-1, 1:400 [ab51872, Abcam]), and transforming growth factor beta 1 (TGF-β1, 1:800 [ab92486, Abcam]). The rationale for examining these molecules is that Osx is expressed in osteoblasts of endochondral and membranous bones (20); VEGFR-1 is a high-affinity receptor for vascular endothelial growth factor produced by endothelial cells during angiogenesis (21); and TGF-β1 influences growth, differentiation, and extracellular matrix (ECM) secretion during bone development (22). Tissue sections were subsequently incubated with horseradish peroxidase–conjugated secondary antibodies using diaminobenzidine (Zhongshan Golden Bridge Biotechnology, Beijing, China) as chromogen.

Matrix Secretion by rBMSCs on Different Scaffolds

To examine the effect of scaffolds on secretion of the ECM, rBMSCs at passage 4 were seeded *ex vivo* at 5×10^4 cells/scaffold ($n = 3$) and cultured with regular medium without any osteogenic supplements at 37°C in 5% CO_2. On days 2 and 14, scaffolds were fixed with 2.5% glutaraldehyde in PBS and lyophilized for scanning electron microscopic examination and energy-dispersive X-ray spectroscopy elemental analysis.

Statistical Analysis

Micro-CT–generated data increased in radiopacity within the critical-sized defect, and new bone formation at the defect margin and defect center derived from histologic evaluation was statistically analyzed. For each parameter, the data sets were analyzed to ascertain that the normality and equal variance assumptions were not violated before the use of 1-way analysis of variance and Holm-Sidak pairwise comparison procedures. If those assumptions were violated, nonlinear transformation of the data sets was performed before use of parametric statistical methods. For all tests, statistical significance was preset at $\alpha = 0.05$.

Results

Scanning electron microscopic images of porous Col-Ap, β-TCP, and Col scaffolds are shown in Figure 1*A*. The elemental compositions of these scaffolds shown in Figure 1*B* confirmed the presence of calcium and phosphorus within the Col-Ap scaffold.

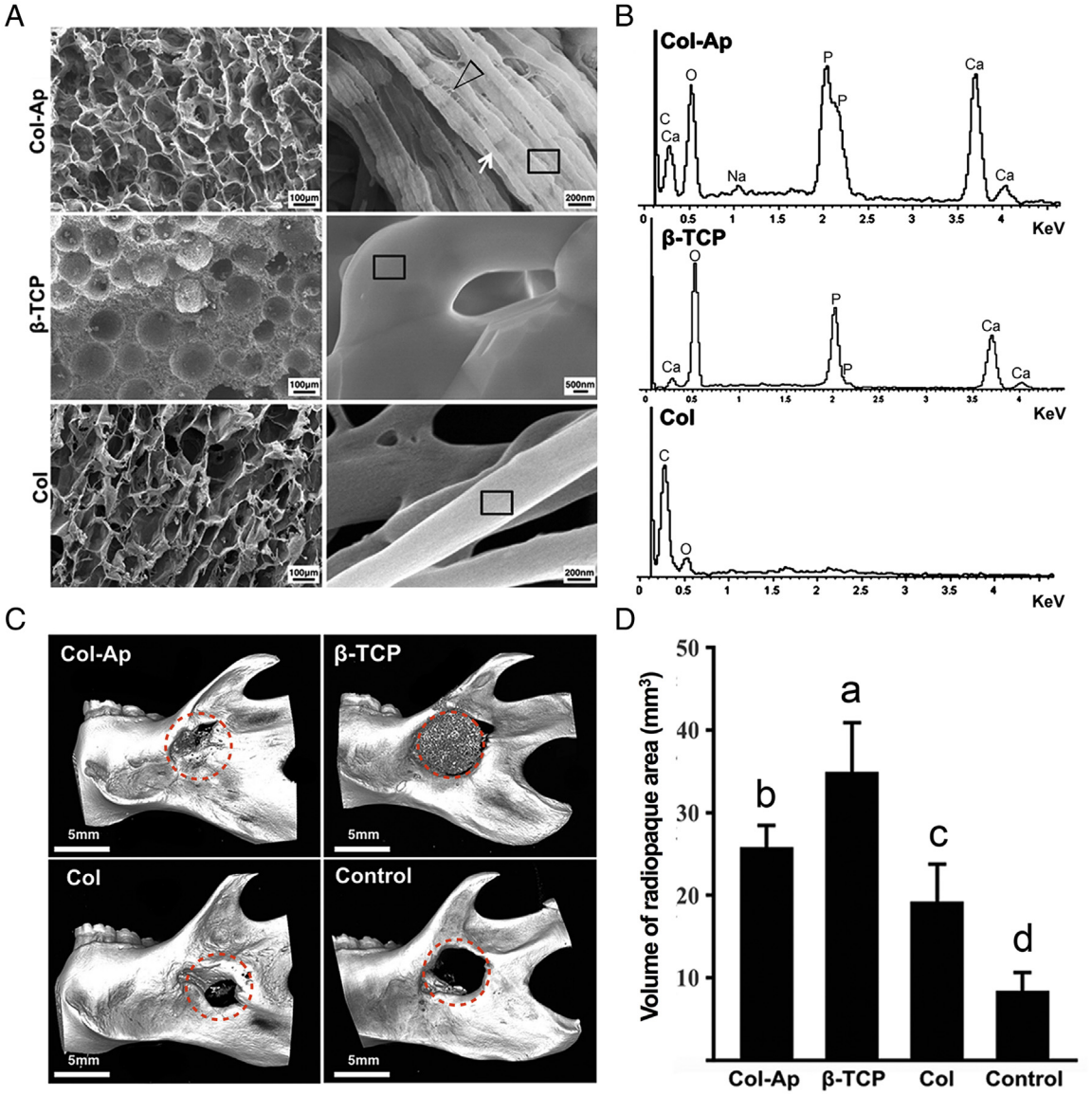

Figure 1. (*A*) Representative (*left*) low- and (*right*) high-magnification scanning electron microscopic images of cross sections of Col-Ap, β-TCP, and Col porous scaffolds. The Col-Ap scaffold (*top*) showed a spongy morphology with a filamentous substructure. The pores were mostly interconnected and evenly distributed, with a pore size of 142.2 ± 25.5 μm. *Arrow*, microfibrils with a diameter of 75.5 ± 8.2 nm; *open arrowhead*, intermolecular cross-links. (*Middle*) The β-TCP scaffold revealed a particlelike morphology, with a macropore size of 138.5 ± 39.5 μm and a micropore size of 2.9 ± 0.9 μm. (*Bottom*) The Col scaffolds (bottom) had macropores of 100.9 ± 6.7 μm. (*B*) Energy-dispersive X-ray spectroscopy of regions of interest (boxes in *A*) in different scaffolds, confirming the presence of apatite crystallites within the microfibrils in the Col-Ap scaffold. (*C*) Representative micro-CT images of the mandibular defect area after implantation with different scaffolds for 20 weeks. (*D*) Volume analysis of the radiopaque area. Groups labeled with different lowercase letters are significantly different ($P < .05$).

After implantation for 20 weeks, bone defects in the Col-Ap group were almost filled with fibrous bone structures even at the defect center, whereas those in the β-TCP group remained radiopaque, and an obvious boundary was observed between the scaffold and defect margin. By contrast, only a small amount of bone was formed along the defect margin in the Col group, whereas the defect area of the control group was not altered (Fig. 1*C*). Quantitative analysis of the micro-CT results based on radiopacity alone indicated that the β-TCP group apparently achieved a significantly higher extent of bone regeneration compared with the Col-Ap group ($P < .05$, Fig. 1*D*).

Histologic analysis of the microstructure of tissues in the defect areas (Fig. 2*A*) shows abundant new bone formation along the defect margin in the Col-Ap group with vascularized structures and osteoblast-like cells. New bone and osteoid with a bone marrow–like structure were also identified at the defect center. Although limited new bone structure could be identified near the defect margin in the β-TCP group, loose connective soft tissues were found at the defect center after decalcification, with unresorbed scaffold remnants. In the Col group, little new bone was seen along the defect margin, and residual Col scaffolds together with connective soft tissues were found at the defect center. Semiquantitative

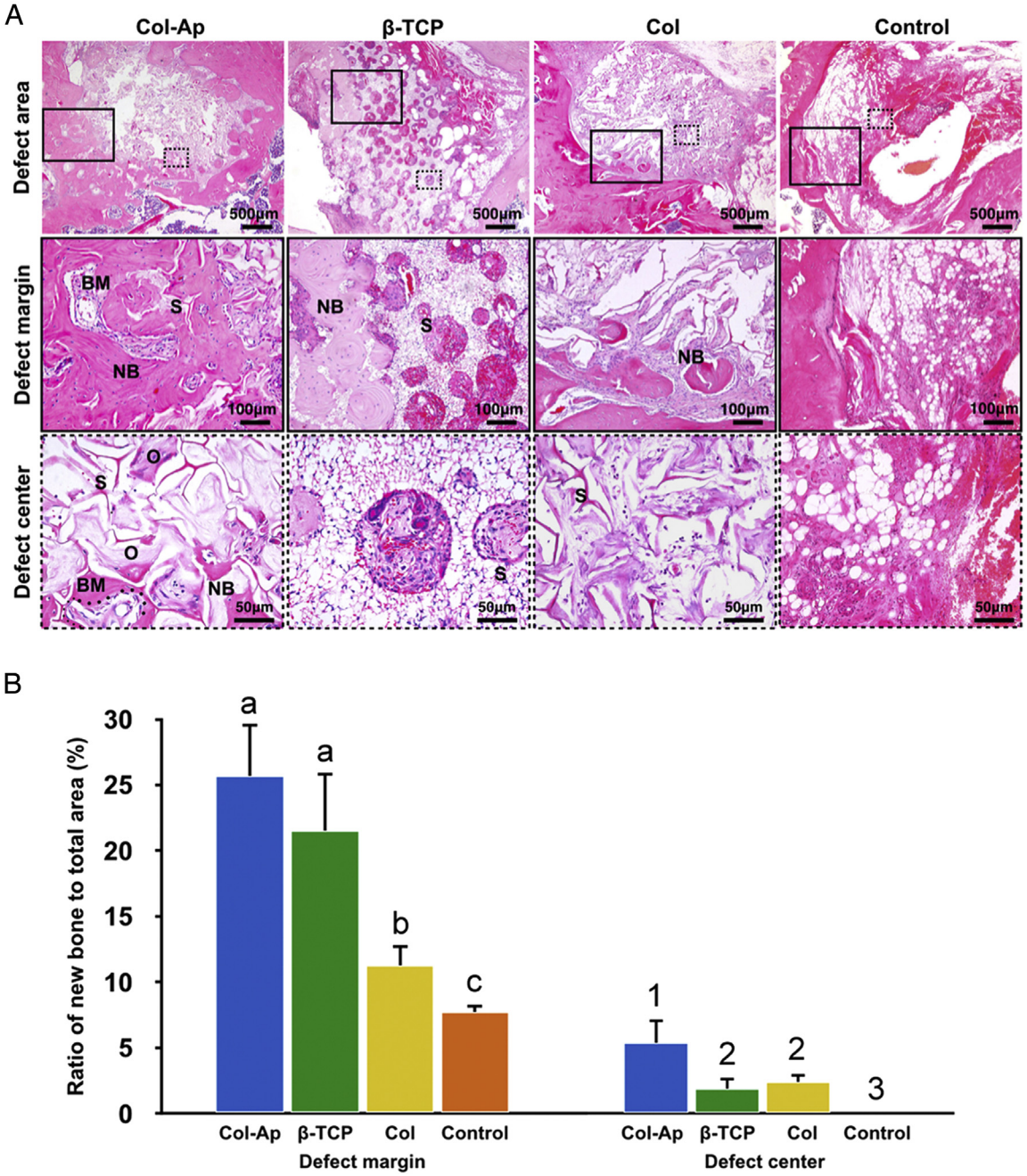

Figure 2. Light microscopy of hematoxylin-eosin–stained sections of mandible defects in the defect margin and defect center of different *in vivo* groups. (*A*) Profuse new bone (NB) and bone marrow (BM) were found in the Col-Ap group, whereas a large amount of remnant scaffold (S) was observed in the β-TCP group. Little new bone with a small amount of residual scaffold was seen in the Col group. O, osteoid. (*B*) Semiquantitative analysis of new bone based on histologic examination ($n = 15$). For the defect margin, groups labeled with the same lowercase letters are not significantly different ($P > .05$). For the defect center, groups labeled with the same numerals are not significantly different ($P > .05$).

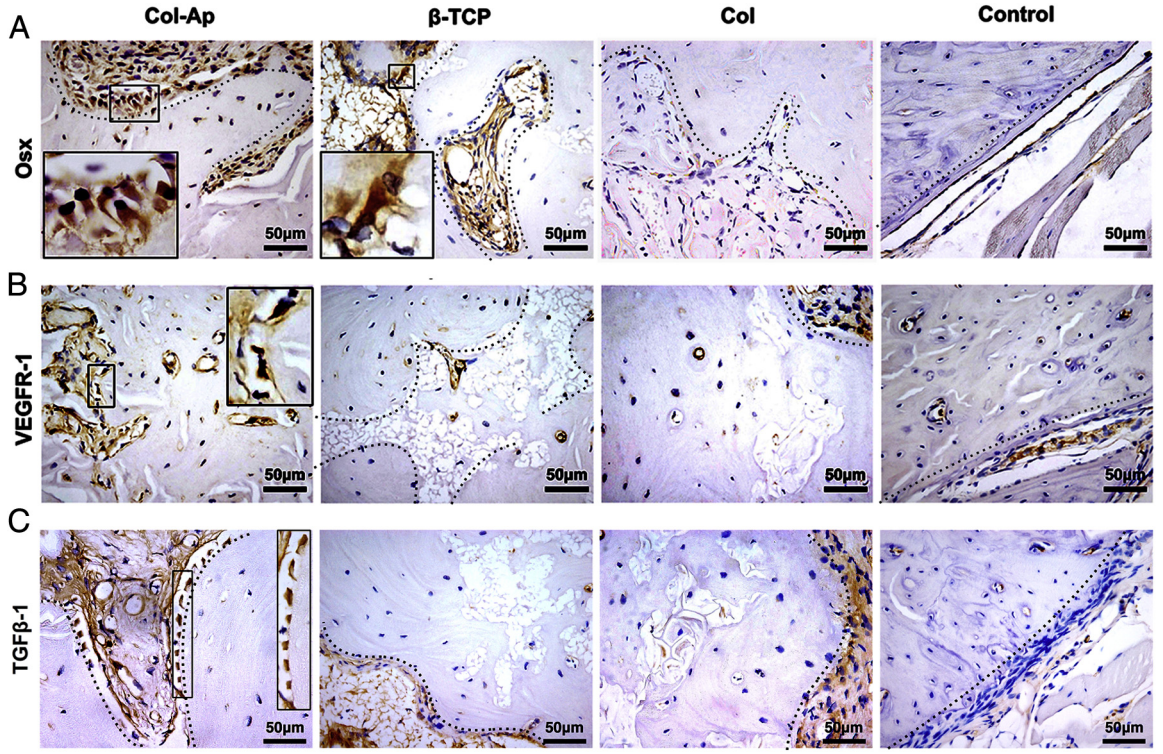

Figure 3. Immunohistochemical staining of (*A*) Osx, (*B*) VEGFR-1, and (*C*) TGF-β1 in the defect areas of the 4 *in vivo* groups.

analysis (Fig. 2*B*) indicated that there was significantly more new bone present in the Col-Ap group compared with the other groups ($P < .05$).

Immunohistologic staining showed that the Col-Ap group exhibited the highest expression level of Osx along the margins of newly formed bone tissues (Fig. 3*A*). The expression level of VEGFR-1 was also higher in the Col-Ap and β-TCP groups when compared with the Col and control groups (Fig. 3*B*). Positive staining of TGF-β1 was found in the defect area of the Col-Ap group, whereas weak or negative staining was identified in the other groups (Fig. 3*C*).

The *ex vivo* osteogenic ability of the scaffolds after seeding with rBMSCs is shown in Figure 4. After 2 days, rBMSCs contacted well in all types of scaffolds via their filopodia (Fig. 4*A*). Secretion of ECM was more extensive in the Col-Ap and Col groups than the β-TCP group, but no sign of matrix mineralization was detectable. On day 14, rBMSCs spread all over the surface of all scaffolds (Fig. 4*B*). In the Col-Ap group, the rBMSCs produced numerous matrix vesicles attached to cell membranes, and the intercellular space was occupied by meshlike ECM. These results were complementary to the *in vivo* immunohistologic staining of TGF-β1 in that the Col-Ap group accumulated the largest amount of ECM. Elemental analysis showed that these ECMs mainly consisted of mineralized Col (Supplemental Figure S2 is available online at www.jendodon.com). The presence of mineralized Col was not apparent in the other 2 groups. Large calcium nodules were deposited on the cell surface in the β-TCP group, whereas a fibrous ECM consisting of carbon and oxygen elements indicative of collagenous matrix secretion was detected in the Col group (Supplemental Figure S2 is available online at www.jendodon.com).

Discussion

Healing of large bone defects in unresolved apical periodontitis is similar to the healing of other surgical defects in the body in that it is necessary to control cell behavior and ECM accumulation (23). To achieve this goal, biomimetic scaffolds that can mimic natural bone ECM provide the most similar microenvironment to nature. Previous attempts in the development of bonelike Col/hydroxyapatite composites focused on the deposition of apatite crystallites around Col fibrils and have only reproduced a similar chemical composition rather than the nanostructure of bone ECM (24). In the present study, a 3D Col-Ap nanocomposite was fabricated using a modified bottom-up biomimetic approach, enabling the formation of bonelike subfibrillar nanostructures at the molecular and nanoscale levels (14, 15). In this strategy, self-assembly of triple-helical tropocollagen molecules into microfibrils and deposition of polyacrylic acid–stabilized amorphous nanoprecursors inside the microfibrils occur simultaneously although such a process does not fully mimic the manner in which natural bone formation occurs. The subfibrillar nanostructures in the Col-Ap nanocomposite provide a large interface area, maximizing the strengthening effects associated with the interactions at the organic-inorganic interface (25).

The design of tissue engineering scaffolds includes 3 general characteristics: biocompatibility with surrounding tissues; degradation rate commensurate with bone remodeling; and adequate porosity to facilitate cell infiltration, nutrient diffusion, and vascularization (26). *Ex vivo* cell seeding of rBMSCs showed attachment and spreading over the Col-Ap nanocomposite, which is indicative of its biocompatibility. In clinical trials of bone regeneration, 4 to 6 months are required for complete biodegradation of resorbable synthetic scaffolds (27). After implantation for 20 weeks, the Col-Ap nanocomposite partially degraded and allowed new bone ingrowth, whereas large amounts of remnant β-TCP existed in the defect area, inhibiting bone healing. The remnant, radiopaque β-TCP particles also increased the apparent volume of regenerated area in defects during micro-CT evaluation. This important issue indicates that histologic analysis is mandatory in evaluating new bone volume. Scaffold porosity and pore interconnectivity are important for cell migration and vascular tissue ingrowth (28); previous studies have shown that pore size between 100 and 400 μm is optimal for

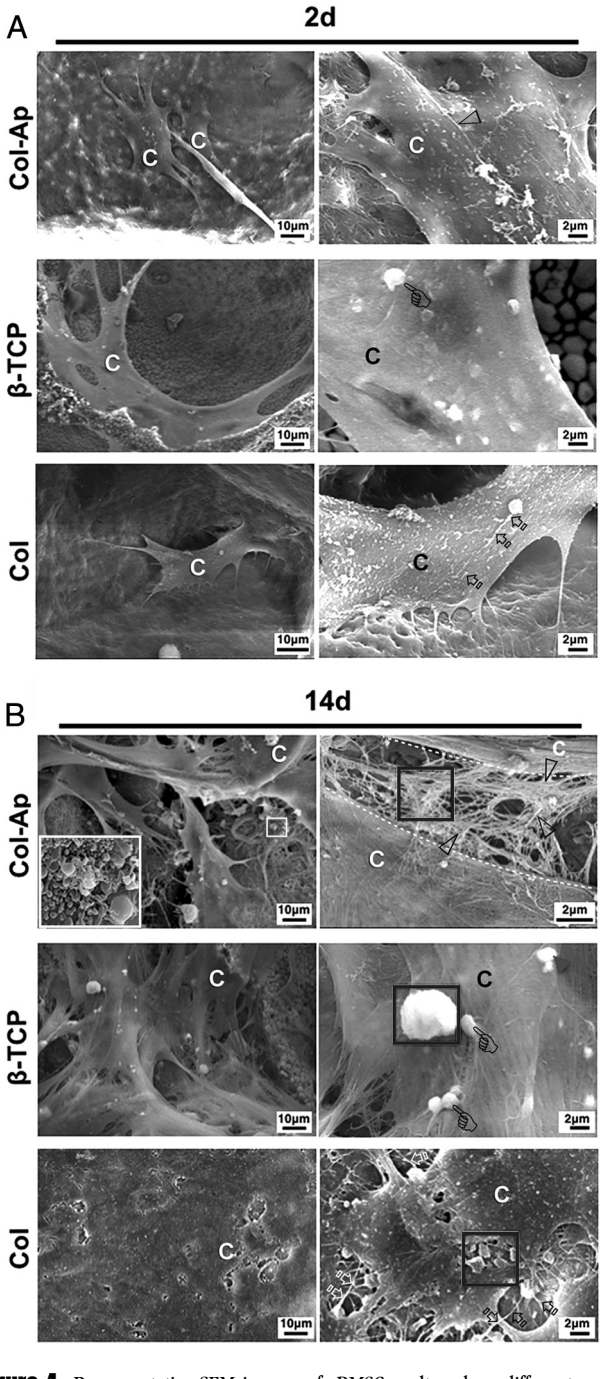

Figure 4. Representative SEM images of rBMSCs cultured on different scaffolds under *ex vivo* conditions. (*A*) On day 2 (2d), rBMSCs attached to all the scaffolds, and ECM was secreted on the cell surface. (*B*) On day 14 (14d), the Col-Ap group showed the most active vesicle secretion (*white box inset*: high magnification of boxed area) with abundant fibrous ECM (*open arrowheads*). Calcified nodules (*pointers*) were observed in the β-TCP group, whereas only a small amount of fibrous ECM was present in the Col groups (*open arrows*). (*C*) rBMSCs. *Black boxes* in the right column were used for EDX analysis (Supplemental Figure S2 is available online at www.jendodon.com).

bone ingrowth (29). The Col-Ap nanocomposite has a pore size of 142.2 $\pm$ 25.5 μm, with more interconnective spaces than β-TCP. Vascular invasion is an important event because it facilitates the influx of osteoblasts, osteoclasts, and hematopoietic cells to form ossification centers (30). A well-developed vascular system with enhanced VEGFR-1 expression is present in the Col-Ap group for delivery of nutrients to support bone healing.

Similar to the formation of the extracellular matrix *in vivo* (31), seeding of rBMSCs on the Col-Ap scaffolds *ex vivo* resulted in secretion of membrane-bound matrix vesicles. It has been shown that amorphous calcium phosphates are present inside these vesicles (32). Disruption of the vesicles enables the amorphous mineral phase to be released to the extracellular spaces (33). Organic components from the ECM regulate the nucleation of extracellular apatite from amorphous calcium phosphate (34). Increased expression of Osx during healing of the *in vivo* defects is an indication of the osteoinductive potential of the Col-Ap nanocomposite. TGF-β1 is an important transcription factor involved in the regulation of matrix formation and mineralization (35). Increased expression of TGF-β1 in the Col-Ap group is suggestive of the involvement of the TGF-β1 signaling pathway in the formation of mineralized ECM induced by the Col-Ap nanocomposite.

Within the limits of the present study, it may be concluded that a Col-Ap nanocomposite that mimics the subfibrillar nanostructure of natural bone possesses noteworthy properties of bone regeneration and vascularization. Because of its maneuverability and adaptability to an irregular surgical site, the Col-Ap nanocomposite may be further developed for clinical applications in bone regeneration of large periapical lesions after apical curettage or apicoectomy wherein part of the surgical defect is blocked by the presence of a partially resected root.

Acknowledgments

The authors thank Ting Zhang and Qing Luo for staining assistance.

Supported by the National Science Foundation of China (No.81571815) and the Beijing Municipal National Science Foundation (No.7152156).

The authors deny any conflicts of interest related to this study.

Supplementary Material

Supplementary material associated with this article can be found in the online version at www.jendodon.com (http://dx.doi.org/10.1016/j.joen.2016.04.027).

References

1. Rud J, Andreasen JO. A study of failures after endodontic surgery by radiographic, histologic and stereomicroscopic methods. Int J Oral Surg 1972;1:311–28.
2. Molven O, Halse A, Grung B. Observer strategy and the radiographic classification of healing after endodontic surgery. Int J Oral Maxillofac Surg 1987;16:432–9.
3. Rubinstein RA, Kim S. Short-term observation of the results of endodontic surgery with the use of a surgical operation microscope and Super-EBA as root-end filling material. J Endod 1999;25:43–8.
4. Skoglund A, Persson G. A follow-up study of apicoectomized teeth with total loss of the buccal bone plate. Oral Surg Oral Med Oral Pathol 1985;59:78–81.
5. Von Arx T, Britain S, Cochran DL, et al. Healing of periapical lesions with complete loss of the buccal bone plate: a histologic study in the canine mandible. Int J Periodontics Restorative Dent 2003;23:157–67.
6. Von Arx T, Alsaeed M. The use of regenerative techniques in apical surgery: a literature review. Saudi Dent J 2011;23:113–27.
7. Corbella S, Taschieri S, Elkabbany A, et al. Guided tissue regeneration using a barrier membrane in endodontic surgery. Swiss Dent J 2016;126:13–25.
8. Fillingham Y, Jacobs J. Bone grafts and their substitutes. Bone Joint J 2016; 98-B(suppl A):6–9.
9. Liu B, Lun DX. Current application of β-tricalcium phosphate composites in orthopaedics. Orthop Surg 2012;4:139–44.
10. Kamitakahara M, Ohtsuki C, Miyazaki T. Review paper: behavior of ceramic biomaterials derived from tricalcium phosphate in physiological condition. J Biomater Appl 2008;23:197–212.
11. Sarikaya B, Aydin HM. Collagen/beta-tricalcium phosphate based synthetic bone grafts via dehydrothermal processing. Biomed Res Int 2015;2015:576532.

12. Wang Y, Azaïs T, Robin M, et al. The predominant role of collagen in the nucleation, growth, structure and orientation of bone apatite. Nat Mater 2012;11:724–33.
13. Chan CK, Kumar TS, Liao S, et al. Biomimetic nanocomposites for bone graft applications. Nanomedicine 2006;1:177–88.
14. Liu Y, Luo D, Kou XX, et al. Hierarchical intrafibrillar nanocarbonated apatite assembly improves the nanomechanics and cytocompatibility of mineralized collagen. Adv Funct Mater 2013;23:1404–11.
15. Liu Y, Luo D, Liu S, et al. Effect of nanostructure of mineralized collagen scaffolds on their physical properties and osteogenic potential. J Biomed Nanotechnol 2014;10:1049–60.
16. Kokubo T, Kushitani H, Sakka S, et al. Solutions able to reproduce *in vivo* surface-structure changes in bioactive glass-ceramic A-W. J Biomed Mater Res 1990;24:721–34.
17. Maniatopoulos C, Sodek J, Melcher AH. Bone formation *in vitro* by stromal cells obtained from bone marrow of young adult rats. Cell Tissue Res 1988;254:317–30.
18. Gronthos S, Mankani M, Brahim J, et al. Postnatal human dental pulp stem cells (DPSCs) *in vitro* and *in vivo*. Proc Natl Acad Sci U S A 2000;97:13625–30.
19. Hollinger JO, Kleinschmidt JC. The critical size defect as an experimental model to test bone repair materials. J Craniofac Surg 1990;1:60–8.
20. Tu Q, Valverde P, Li S, et al. Osterix overexpression in mesenchymal stem cells stimulates healing of critical-sized defects in murine calvarial bone. Tissue Eng 2007;13:2431–40.
21. Stuttfeld E, Ballmer-Hofer K. Structure and function of VEGF receptors. IUBMB Life 2009;61:915–22.
22. Janssens K, Ten Dijke P, Janssens S, et al. Transforming growth factor-beta1 to the bone. Endocr Rev 2005;26:743–74.
23. Dimitriou R, Jones E, McGonagle D, et al. Bone regeneration: current concepts and future directions. BMC Med 2011;9:66.
24. Ma PX. Biomimetic materials for tissue engineering. Adv Drug Deliv Rev 2008;60:184–98.
25. Li Y, Aparicio C. Discerning the subfibrillar structure of mineralized collagen fibrils: a model for the ultrastructure of bone. PLoS One 2013;8:e76782.
26. Polo-Corrales L, Latorre-Esteves M, Ramirez-Vick JE. Scaffold design for bone regeneration. J Nanosci Nanotechnol 2014;14:15–56.
27. Sotome S, Ae K, Okawa A, et al. Efficacy and safety of porous hydroxyapatite/type 1 collagen composite implantation for bone regeneration: a randomized controlled study. J Orthop Sci 2016;21:373–80.
28. Jafari M, Paknejad Z, Rad MR, et al. Polymeric scaffolds in tissue engineering: a literature review. J Biomed Mater Res B Appl Biomater 2015 Oct 23; http://dx.doi.org/10.1002/jbm.b.33547 [Epub ahead of print].
29. Murphy CM, Haugh MG, O'Brien FJ. The effect of mean pore size on cell attachment, proliferation and migration in collagen-glycosaminoglycan scaffolds for bone tissue engineering. Biomaterials 2010;31:461–6.
30. Portal-Núñez S, Lozano D, Esbrit P. Role of angiogenesis on bone formation. Histol Histopathol 2012;27:559–66.
31. Anderson HC, Garimella R, Tague SE. The role of matrix vesicles in growth plate development and biomineralization. Front Biosci 2005;10:822–37.
32. Wuthier RE, Lipscomb GF. Matrix vesicles: structure, composition, formation and function in calcification. Front Biosci (Landmark Ed) 2011;16:2812–902.
33. Boonrungsiman S, Gentleman E, Carzaniga R, et al. The role of intracellular calcium phosphate in osteoblast-mediated bone apatite formation. Proc Natl Acad Sci U S A 2012;109:14170–5.
34. Gajjeraman S, Narayanan K, Hao J, et al. Matrix macromolecules in hard tissues control the nucleation and hierarchical assembly of hydroxyapatite. J Biol Chem 2007;282:1193–204.
35. Zhou S. TGF-β regulates β-catenin signaling and osteoblast differentiation in human mesenchymal stem cells. J Cell Biochem 2011;112:1651–60.